# Modeling the Electrical Behavior of Anatomically Complex Neurons Using a Network Analysis Program: Passive Membrane

I. Segev[1,2,**], J. W. Fleshman[1], J. P. Miller[2,*], and B. Bunow[3]

1 Mathematical Research Branch, National Institute of Arthritis, Diabetes, and Digestive and Kidney Diseases, Bldg. 31, Rm. 4B54
2 Laboratory of Neural Control, National Institute of Neurological and Communicative Disorders and Stroke, Bldg. 36, Rm. 5A29
  National Institutes of Health, Bethesda, MD 20205, USA
3 Laboratory of Applied Studies, Division of Computer Research and Technology, Bldg. 12A, Rm. 2045

**Abstract.** We describe the application of a popular and widely available electrical circuit simulation program called SPICE to modeling the electrical behavior of neurons with passive membrane properties and arbitrarily complex dendritic trees. Transient responses may be calculated at any location in the cell model following current, voltage or conductance perturbations at any point. A numbering method is described for binary trees which is helpful in transforming complex dendritic structures into a coded list of short cylindrical dendritic segments suitable for input to SPICE. Individual segments are modeled as isopotential compartments comprised of a parallel resistor and capacitor, representing the transmembrane impedance, in series with one or two core resistors. Synaptic current is modeled by a current source controlled by the local membrane potential and an "alpha-shaped" voltage, thus simulating a conductance change in series with a driving potential. Extensively branched test cell circuits were constructed which satisfied the equivalent cylinder constraints (Rall 1959). These model neurons were perturbed by independent current sources and by synaptic currents. Responses calculated by SPICE are compared with analytical results. With appropriately chosen model parameters, extremely accurate transient calculations may be obtained. Details of the SPICE circuit elements are presented, along with illustrative examples sufficient to allow implementation of passive nerve cell models on a number of common computers. Methods for modeling excitable membrane are presented in the companion paper (Bunow et al. 1985).

## 1 Introduction

The role of dendritic geometry in the integrative function of nerve cells has been studied extensively over the last three decades, both analytically and through the use of computational models (see Rall 1977, for review). These studies have created the conceptual and mathematical tools needed to answer precise questions about the connection between neuronal form and function. Recent advances in cell staining techniques, most notably the introduction of horseradish peroxidase (e.g. Cullheim and Kellerth 1976; Jankowska et al. 1976), have enabled physiological study of neurons which may subsequently be visualized in exquisite morphological detail. If physiological and anatomical measurements are made on the same cell, then quantitative computer models may reveal how the physiological domain is mapped onto the morphological domain.

To study the mechanisms by which a neuron processes its synaptic inputs, the cable properties of the postsynaptic neuron as well as the anatomical and physiological characteristics of the synaptic inputs must be known. Rall (1959, 1960, 1962, 1967, 1969) has developed a theoretical basis to derive these properties using data obtained from intracellular recording. Other analytical models of nerve cells have been developed by Jack and Redman (1971); Barrett and Crill (1974); Butz and Cowan (1974); Poggio and Torre (1977) and Horwitz (1981).

These analytical approaches assumed passive membrane properties and were limited by practical computational concerns to very small numbers of synaptic inputs. If one is interested in morphologically complex cells and in nonlinear membrane events, such as synaptic conductance changes, rectification or spike generation, a compartmental model is appropriate, and, for certain problems, mandatory (Rall 1964). In the compartmental approach, the neuron is

* *Present address:* Department of Zoology, University of California, Berkeley, CA 94720, USA
** *Present address:* Department of Neurobiology, Institute of Life Sciences, The Hebrew University, Jerusalem, Israel

disassembled into regions or compartments of membrane small enough to be considered isopotential which, therefore, may be represented by a membrane capacitance in parallel with a membrane resistance. Series resistors connect adjacent compartments (Rall 1964; Perkel and Mulloney 1978a, b). The continuous cable equation, a second order, partial differential equation, is thus approximated by a system of ordinary differential equations. The advantage of this approach is that it places no restrictions on the membrane properties of each compartment (e.g. compartments may be passive or excitable) or on the geometry of the neuron.

Several groups have used compartmental approaches to simulate the electrical behavior of neurons (passive models, e.g. Rall 1964; Rall et al. 1967; Brown et al. 1981; Edwards and Mulloney 1984; active models, e.g. Cooley and Dodge, 1966; Rall and Shepherd 1968; Khodorov 1974; Goldstein and Rall 1974; Moore et al. 1975; Traub and Llinas 1979; Parnas and Segev 1979). However these compartmental models did not approach the anatomical and physiological complexity of real nerve cells. For example, cat α-motoneurons may have a dozen or more dendrites, which may bifurcate as many as ten times before terminating (Ulfhake and Kellerth 1981; Cullheim et al. 1985). Realistic representation of such cells may require thousands of compartments (Fleshman et al., in preparation; Shelton 1985) and, therefore, the simultaneous solution of thousands of differential equations.

Fortunately for those of us who would model nerve cells, electrical network analysis programs exist which are capable of handling circuits of this complexity, as first suggested by Shepherd and Brayton (1979). One such program is called SPICE, a general purpose circuit simulation program developed in the Department of Electrical Engineering and Computer Sciences at the University of California, at Berkeley (Vladimirescu et al. 1981). SPICE is an inexpensive FORTRAN program which can be run on several widely available computers, from the CDC Cyber to the DEC VAX 11/750 to the IBM PC-XT (see Bunow et al. 1985; upon request, the authors will provide information about how to obtain copies of SPICE). As we will show in this paper, SPICE is readily applied to study the behavior of passive, arbitrarily complex neurons in response to current pulses and synaptic currents. Modeling nonlinear and excitable membrane properties is the subject of the following paper.

The plan of this paper is as follows: Section 2 discusses the representation of a dendritic neuron as a spherical soma and a coded collection of short cylindrical segments. The basic approach employed in SPICE to describe electrical circuits is described. Then circuit

analogues are developed for the cell soma, dendritic segments, independent current and voltage sources and synapses using the SPICE format. In Sect. 3, idealized test cells are constructed and the performance of the computer models is compared against analytical results. Some numerical and related convergence problems are considered.

## 2 Model Formulation

### 2.1 Reduction of Complex Dendritic Trees to Simple Units

The transformation of a complex dendritic neuron into an equivalent network of discrete electrical components may be accomplished by "disassembling" the cell into a spherical soma and a set of interconnected cylindrical dendritic segments of known length and diameter (Rall 1959; Barrett and Crill 1974). In dealing with the large α-motoneurons of the cat spinal cord (Cullheim et al. 1985; Fleshman et al., in preparation) we have found it useful to devise a system of nomenclature which uniquely describes the position of every segment in the dendritic arborization.

The naming system, illustrated in Fig. 1A, is based on a symmetrically branched binary tree. The figure shows a hypothetical dendrite (solid lines) superimposed on a fully branched tree (dotted lines). The stem dendrite, defined as branch order zero, bifurcates into 2 first order daughter branches, which bifurcate into 4 second order daughter branches. Of the second order branches, branches 1, 3 and 4 continue to bifurcate, but branch 2 terminates. Note that the numbering of third order branches of the hypothetical dendrite is the same as for the fully branched tree, even though the third order branches numbered 3 and 4 are missing. Thus, in this system, the order of daughter branches is one greater than the parent's, the branch number of the right-hand daughter is twice the parent's branch number and the number of the left hand daughter is one less than the right.

Figure 1B, C shows the application of this naming system to a dendrite from an HRP-filled motoneuron. The anatomical dendrite in B is represented in C as an appropriately scaled binary dendrogram. The names of all of the dendritic branches from the stem, branch 0001, to terminal branch 6011, are also shown. In Fig. 1C arrow heads indicate points at which dendritic branches are subdivided into shorter cylindrical segments.

The diameters of real dendrites are not necessarily uniform between branch points (Barrett and Crill 1974; Cullheim et al. 1985). We applied a sampling rule whereby branches less than 500 μm long were divided in half and branches longer than 500 μm were divided into 200 μm long segments beginning at the proximal
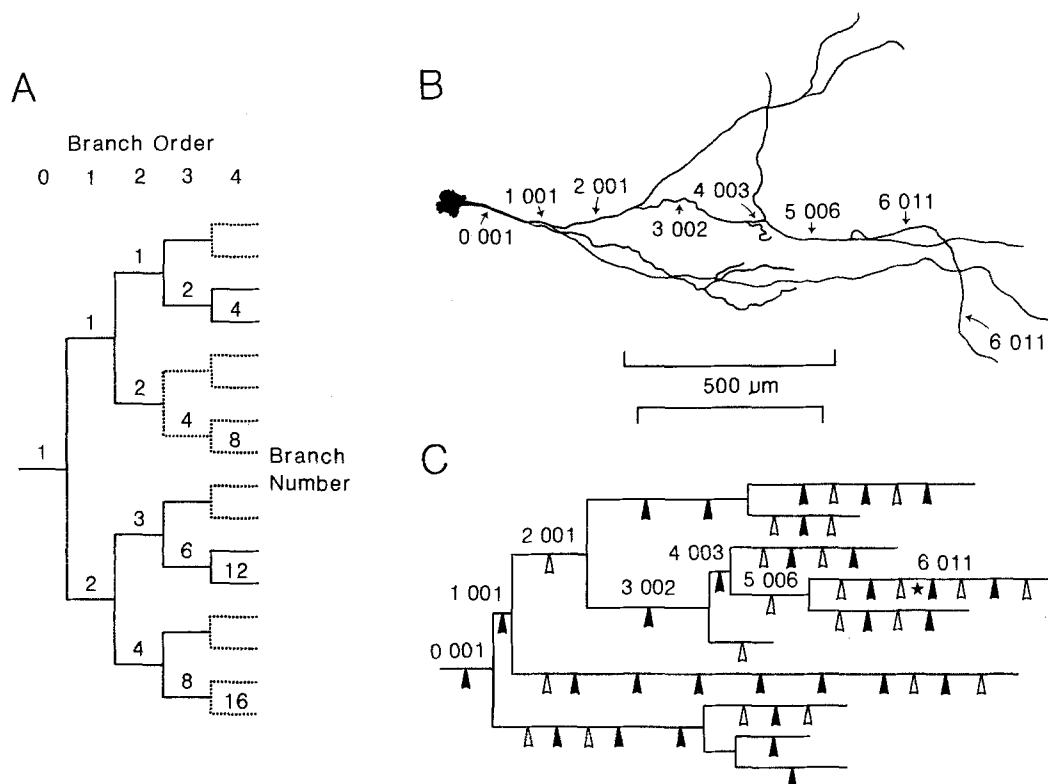
**Fig. 1A–C.** A system of nomenclature for binary dendritic branching. **A** Archetypal dendritic tree symmetrically branched to the fourth order (dotted), with an asymmetrical dendrite superimposed (solid line). Note that "missing" branch numbers are still counted. **B** Reconstruction of an HRP-filled α-motoneuron dendrite, with branch names along the path from soma to sixth order terminal branch 011. **C** Dendrogram of dendrite in B, showing initial anatomical branch segmentation (filled arrows) and subsequent electrotonic segmentation (empty arrows) for $R_m = 7000\,\Omega\,cm^2$ and $R_i = 70\,\Omega\,cm$

branch point. Diameter measurements were made at the midpoint of each segment (see Cullheim et al. 1985 for details of anatomical methods). This initial segmentation is shown in Fig. 1C by the filled arrow heads.

The electrical length of a dendritic cylinder depends on the anatomical length and diameter of the segment, as well as the specific membrane ($R_m$) and cytoplasmic ($R_i$) resistivities. As discussed below, the accuracy of an electrical circuit model depends, in part, on the electrical length of individual segments. In order to keep the electrical length of all segments less than a criterion value ($0.2\lambda$) for a particular choice of $R_m$ and $R_i$, it was necessary to further divide some of the segments, as shown by the empty arrows in Fig. 1C. Segments were numbered, beginning with zero, and this number completed the segment name. For example, if the dendrite shown in Fig. 1 is dendrite 4, the complete name of the segment marked by the asterisk in C would be 4601103.

### 2.2 Basic Circuit Elements

Here we describe some basic techniques for modeling passive nerve cells with SPICE. The information presented here is not intended to supplant the SPICE

manual, but rather may serve as a neuron-specific addendum to it.

SPICE input takes the form of a "wiring list", in which each element of the network is connected to two or more nodes, just as one would solder a real element onto a circuit board. The usual elements of electrical networks are provided in SPICE: resistors, capacitors, voltage and current sources, and even semiconductor elements such as diodes and transistors. Each element in the circuit must have a unique name, the first character of which defines the element type. For the purposes of this paper, only resistors (R), capacitors (C), independent current (I) and voltage (V) sources and voltage-controlled current sources (G) are needed. The remaining characters of the name (up to eight total) are numbers or letters. Following the name are the integer numbers of the nodes to which the element is attached. Node 0 has a special meaning in SPICE, representing system ground. Lastly, the special characteristics of the element are indicated, such as the resistance of a particular resistor. For example an R–C block to ground could be written as

```
R1    1    0    1MEG
C1    1    0    1PF.
```

In addition to describing circuit topology, the user may specify one of several analysis modes, such as AC small signal, DC or transient analyses.

### 2.2.1 Passive Isopotential Compartment.

Three basic neuronal components may be represented in SPICE as passive isopotential compartments: the soma, the nonterminal dendritic segment and the terminal dendritic segment. In Fig. 2A, a schematic representation (left column) and the equivalent electrical circuit (middle column) for the soma is shown. Here RM and CM are the membrane resistance and membrane capcitance. These values are related to the specific $R_m$ and $C_m$ values as follows

$$RM = R_m/(\pi d_s^2),\tag{1}$$

$$CM = C_m \pi d_s^2,\tag{2}$$

where $d_s$ is the diameter of the soma.

In the right column of Fig. 2A, SPICE input data representing a soma compartment is shown. The values of the soma resistance and capacitance were calculated from Eqs. (1) and (2) assuming $R_m = 10,000\,\Omega\,cm^2$, $C_m = 1\,\mu F/cm^2$ and $d_s = 50\,\mu m$. To inject a current pulse into the soma, an "I" element may also be added, as shown in the third line of the SPICE input data of Fig. 2A. In this way, a depolarizing pulse of 1 nA and a duration of 0.5 ms is applied intracellularly. Current onset is delayed 0.1 ms from the first time point at which membrane potential is computed.

A dendritic segment may be represented by three circuit elements (Fig. 2B, middle column) or four (Fig. 2C, middle column). In both cases the membrane capacitance and the membrane resistance of the whole segment are lumped as single RM and CM values. In the 3-element model, the axial resistance (RI) of the entire segment is placed on one (left) side of the RM–CM elements. In the 4-element representation, the axial resistance is split in half $(RI1 = RI2 = RI/2)$ and the membrane elements are placed at the midpoint of the segment. For a cylindrical segment with a diameter of $d$ cm and a length of $\Delta x$ cm, the RM, CM and RI values are calculated as follows (Rall 1977)

$$RM = R_m/(\pi d\Delta x),\tag{3}$$

$$RI = 4R_i \Delta x/(\pi d^2),\tag{4}$$

$$CM = C_m \pi d\Delta x.\tag{5}$$

SPICE input data for the 3-element and the 4-element representations of a dendritic segment are shown in the right column of Fig. 2B, C. The values of RM, RI, and CM were calculated using Eqs. (3)–(5) for $d = 2.5\,\mu m$, $\Delta x = 100\,\mu m$ and $R_i = 70\,\Omega\,cm$, with $R_m$ and $C_m$ as above. For these parameters the length constant $(\lambda = 1/2(dR_m/R_i)^{1/2})$ is 945 μm and thus the electrical length $(\Delta X = \Delta x/\lambda)$ of the segment is 0.106. As shown below, the 3-element model is somewhat less accurate in predicting the electrical behavior of model neurons, but is more efficient in its use of computer resources. A dendritic terminal is always represented using the 3-element model (Fig. 2B, bottom cylinder on the left
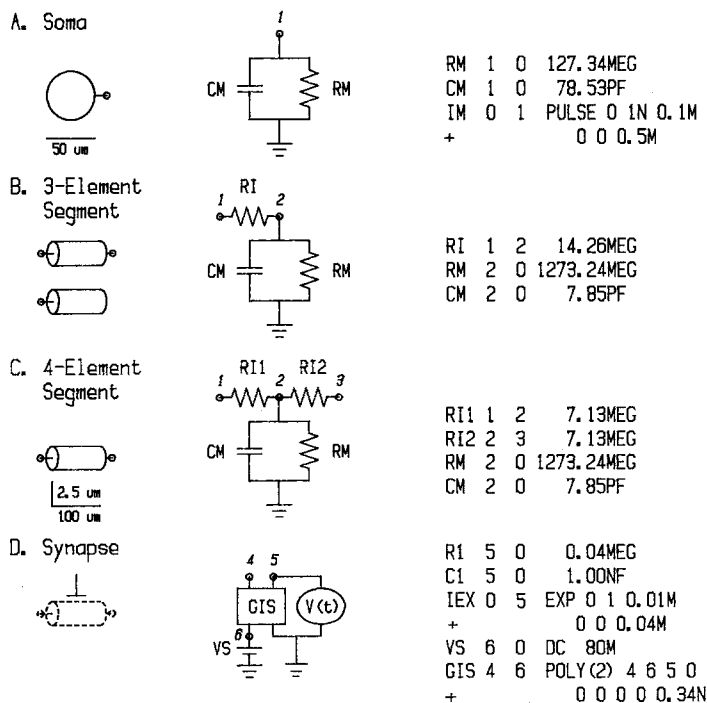


**A. Soma**

```
RM  1  0   127.34MEG
CM  1  0    78.53PF
IM  0  1   PULSE 0 1N 0.1M
+               0 0 0.5M
```

**B. 3-Element Segment**

```
RI  1  2    14.26MEG
RM  2  0  1273.24MEG
CM  2  0     7.85PF
```

**C. 4-Element Segment**

```
RI1 1  2     7.13MEG
RI2 2  3     7.13MEG
RM  2  0  1273.24MEG
CM  2  0     7.85PF
```

**D. Synapse**

```
R1  5  0    0.04MEG
C1  5  0    1.00NF
IEX 0  5   EXP 0 1 0.01M
+              0 0 0.04M
VS  6  0   DC 80M
GIS 4  6   POLY(2) 4 6 5 0
+              0 0 0 0 0.34N
```

**Fig. 2A–D.** Transformation from anatomical entities (soma, dendritic segments, synapse; left column) to equivalent circuits (middle column) to SPICE input code (right column)

column). Individual dendritic branches are represented by a straight chain of dendritic segments. Branch points are represented by three dendritic segments connected to a common node.

*2.2.2 Synaptic Input Circuit.* Synaptic input is commonly modeled as a time varying ("alpha function") conductance change, $g_s(t)$, in series with a synaptic battery, $V_s$ (Rall 1967). Although SPICE does not contain time-varying conductance elements, one may use the elements available in SPICE to design circuits with the desired behavior. The approach used in this paper and the next (Bunow et al. 1985) consists of two steps. First, following a suggestion from Rall, we find a differential equation whose solution is a function with the desired shape. In devising a synapse circuit, the desired shape is the alpha function. Second, an electrical circuit is designed which implements the equation (i.e. the voltage or current output of the circuit has the intended shape). To model a synapse, the synaptic current source is controlled by the alpha function voltage and by the potential at the synapse.

The first step is to write a differential equation whose solution is an alpha function of the form

$$V(t) = At \exp(-t/T_p),\qquad(6)$$

where $T_p$ is the time to peak of $V(t)$ and $A$ has units of V/s.

This equation is the solution of the differential equation

$$\frac{dV}{dt} = (-1/T_p)V + A\exp(-t/T_p),\qquad(7)$$

with $V(0) = 0$.

The SPICE library contains an exponential independent current source which is composed of the sum of two exponentials and is represented as

*IEX N1 N2 N2 EXP (I1 I2 ΔT1 T1 ΔT2 T2)*,

where $N1$ and $N2$ are the connecting nodes and $I1$, $\Delta T1$, $T1$, $I2$, $\Delta T2$, $T2$ are the values, delays and time constants of the first and the second exponents, respectively. By setting $I1 = 0$, $T1 = 0$ and $\Delta T2 = 0$, an exponentially decaying current with a delay of $\Delta T1$, a decay time constant of $T2$ and an initial value of $I2$ is applied between nodes $N1$ and $N2$.

The first three lines in the SPICE input format of Fig. 2D (right) create a circuit model which implements Eq. (7). The current between node 5 and ground in this figure obeys the following equation:

$$C1\frac{dV}{dt} = \frac{-V}{R1} + I2\exp(-t/T2),\qquad(8)$$

where $A$ of Eq. (7) corresponds to $I2/C1$.

Note that in order to obtain a correct "alpha function" (Eq. (6)) from this circuit, care must be taken that $T_p = C1R1 = T2$. In the example of Fig. 2D, a voltage, $V(t)$, with an "alpha function" shape and a time to peak of 0.04 ms is produced at node 5. Note also from Eq. (6) that the voltage peak $V(T_p) = AT_p/\exp(1)$. Substituting $T2$ for $T_p$ and $I2/C1$, for $A$, we obtain

$$V(T_p) = I2R1/\exp(1)\qquad(9)$$

Hence, in the example of Fig. 2D, the alpha function peak amplitude at node 5 is $1.47E4$ V.

The second step in modeling a synapse is to use a voltage dependent current source element ("$G$") in order to produce a synaptic current, $I_s(t)$, of the form

$$I_s(t) = g_s(t)(V_m(t) - V_s),\qquad(10)$$

where $V_s$ is the synaptic equilibrium potential and $V_m(t)$ is the membrane potential at the synapse. The representation of the G element in SPICE is

GIS $N1$ $N2$ POLY(2) $N3$ $N4$ $N5$ $N6$ $p_0$ $p_1$ $p_2$...

where $N1$ and $N2$ are the output nodes; POLY(2) indicates a polynomial in two variables (i.e. two pairs of controlling nodes, $N3$–$N3$ and $N5$–$N6$); and $p_0$, $p_1$,... are the coefficients of the polynomial. For the GIS element above, the current output between node $N1$ and $N2$ is

$$GIS(N1, N2) = p_0 + p_1V(N3, N4) + p_2V(N5, N6)$$
$$+ p_3V^2(N3, N4)$$
$$+ p_4V(N3, N4)V(N5, N6).$$

If $N1$ is the same node as $N3$ and $N2$ is the same as $N4$, a nonlinear resistor is simulated. If the membrane impedance is connected between $N3$ and ground and the synaptic battery is connected between $N4$ and ground, then the controlling voltage $V(N3, N4)$ is equivalent to the $V_m(t) - V_s$ term of Eq. (10). If the alpha function appears between controlling nodes $N5$ and $N6$ and if $p_4$ is the only non-zero coefficient in the polynomial, then the current which flows through this nonlinear resistor has the characteristics of the synaptic current described by Eq. (10).

For the GIS element described by the SPICE data in Fig. 2D (right), the $p_4$ coefficient is $0.34E-9$. Therefore the "synaptic current" is the product of the synaptic conductance change, $0.34E-9[V(5,0)]$ Siemens, and the driving potential, $V(4,6)$. For the parameters of Fig. 2 the peak conductance is approximately $5\,\mu S$. This maximum occurs at $T_p = 0.04$ ms. If this synaptic compartment is connected to a segment with a time constant of 1 ms, it produces a conductance change with $\alpha = 25$ (see Rall 1967; Jack and Redman 1971).

## 3 Model Performance

The critical test of a computer model is to simulate idealized cases for which analytical solutions exist. For example, Rall (1959) defined a class of dendritic structures which are electrically equivalent to a single cylinder. For such "equivalent cylinder neurons", two types of analytical solutions of the one dimensional cable equation were derived: 1) the voltage change, measured at the soma, produced by a brief current injection in the soma (Rall 1959, 1960, 1969) and 2) the voltage response anywhere in the dendritic tree to current injection from an independent source (Rall and Rinzel 1973; Rinzel and Rall 1974; see also Butz and Cowan 1974; Horwitz 1981, 1983) or from a synapse (Rinzel and Rall 1974; Poggio and Torre 1977) at a point in the tree. In the following sections we compare SPICE calculations to the analytical solutions of these two cases.

### 3.1 Independent Current Sources

*3.1.1 Looking from the Soma.* The passive decay of potential, V(t), which results from current injection at the soma of a dendritic structure is a sum of exponential decays such that

$$V(t) = \sum_{i=0}^{\infty} C_i \exp(-t/\tau_i),$$ (11)

where $\tau_0$ equals the membrane time constant, $\tau_m$. When the dendritic structure may be reduced into a single cylinder with an electrical length, $L$, and sealed ends, then (from Rall 1969)

$$L = \frac{\pi}{(\tau_0/\tau_1 - 1)^{1/2}}.$$

By plotting $\log V(t)$ vs $t$ it is possible to obtain $\tau_0$ and $\tau_1$, and thus $L$, graphically by using Rall's "peeling" method.

Our approach to obtain $\tau_0$ and $L$ from the voltage transient calculated by SPICE was to fit the data with a function which is a sum of four decaying exponents (four time constants and the corresponding coefficients, a total of eight free parameters). For this purpose we used a curve-fitting program called MLAB, developed for the DEC System 10 facility at the NIH, which implements a Marquardt-Levenberg curve fitting algorithm (Knott 1979). This method was very satisfactory in obtaining the correct $\tau_0$ and $L$ values from artificial data calculated using the function in Eq. (11) and values for the coefficients and time constants derived analytically for $L$ between 0.5 and 3 (Rall 1969; de Jongh and Kernell 1982). We found that in order to fit the 8 parameters of the function with less than 1% error in $\tau_0$ and $L$, a total number of 500 equally spaced time points with a total duration of $5\tau_0$ is needed. To measure the input resistance at any point in the dendritic structure, we used either a long (steady-state) current pulse or an AC analysis procedure available in SPICE. The latter procedure gives the input impedance at a

circuit node for a specified frequency, in this case a frequency so low (0.1 Hz) that AC impedance approaches DC resistance.

To evaluate the accuracy of transients calculated by SPICE against analytical results, we constructed a test cell similar to a cat spinal α-motoneuron in terms of input resistance ($R_N$), electrical length, time constant and physical dimensions (test-cell 1). This cell was composed of ten identical dendrites, all connected to a common node (the "soma"). Each dendrite formed a binary tree of the fourth order (Fig. 1A) and obeyed the 3/2 power rule at every branch point (Rall 1959). Each dendritic stem (0 order branch) was 10 μm in diameter and 150 μm long. The lengths of the first through fourth order branches were 150, 250, 300, and 450 μm, respectively. Thus the total length of each dendritic path (from soma to terminal) was 1200 μm. We assumed a specific membrane resistance of 7000 Ω cm², a specific axoplasmic resistance of 70 Ω cm and a specific capacitance of 1 μF/cm². Such a dendrite is electrically equivalent to a single cylinder with a diameter of 10 μm, length of 2311 μm, time constant of 7 ms, electrical length of 1.462, and an input resistance of 15.7 MΩ. With a negligibly small soma, the whole "cell" therefore had an input resistance of 1.57 MΩ.

Test-cell 1 was transformed into SPICE input data, using the procedures described above, with a maximum electrical length criterion for each compartment of 0.2λ. This resulted in a total of 1190 compartments. Throughout this study, the SPICE program (version 2G0) was run on a VAX-11/750, operating under VMS, with Floating Point Accelerator hardware and 3.5 Mbytes of memory.

Table 1 compares analytical results with the transients computed using 3-element and 4-element models (Fig. 2). It can be seen that the 4-element model, with $\Delta X \leq 0.2$, gives very accurate results while the 3-element model is correct within 6% (it is noteworthy that $\tau_m$ is well fit with both models, even with longer $\Delta X$ criteria). However, the 3-element model used about half as much CPU time. For some of the cat spinal α-motoneurons we have modeled (Fleshman et al., in

**Table 1.** Comparison between analytical results and SPICE results for test-cell 1 using 3- and 4-element representations of dendritic segments[a]

| Parameter | $R_N$ (MΩ) | $\tau_m$ (ms) | $L$ | CPU time (min) |
|---|---|---|---|---|
| Analytical | 1.57 | 7.00 | 1.46 | |
| 3-Element | 1.67 (+6) | 6.99 (0) | 1.39 (−5) | 20 |
| 4-Element | 1.57 (0) | 6.99 (0) | 1.43 (−2) | 43 |

[a] Numbers in parentheses are percent errors relative to analytical results

preparation) the differences in CPU time required by the two models were much more pronounced, while the differences between the derived parameters $R_N$, $\tau_m$ and $L$ were generally less than 5%. In one extreme case, computing a voltage transient at 500 time points with the 4-element model took 30 h of CPU time, while the same cell required only 16 min with the 3-element model.

Figure 3 shows a 500 point transient calculated by SPICE for a 0.5 ms, 100 nA current pulse injected at the soma of the 4-element representation of test-cell 1. The left ordinate is linear and the right one is logarithmic. The dashed line on the logarithmically scaled transient shows the slowest exponential decay found by the fitting procedure described above. A simple exponential decay, indicating uniform membrane polarization, was reached after about 10 ms ($\sim 1.5\tau_0$). The fitted $\tau_0$ corresponds very closely to the analytical one, as does the fitted $\tau_1$ (and thus $L$) value (Table 1). The transient produced by SPICE for the 3-element model was superimposable, within the thickness of the plotter's pen, on the 4-element transient.

The resistances and capacitance of each compartment are calculated from the length, diameter and specific membrane properties of the corresponding dendritic segment, and there is no a priori requirement that those properties be constant from one compartment to the next. Indeed, in modeling cat spinal $\alpha$-motoneurons we have found that $R_m$ is not uniform, but increases with distance from the soma. Test-cell 1 was used to test the performance of the SPICE program in one such case. Specific membrane resistance was assumed to increase in a sigmoidal fashion from $250\,\Omega\,cm^2$ at the point soma to $40,500\,\Omega\,cm^2$ at the most distal segments. Within a segment, of course, $R_m$ is constant (Fig. 4).

The electrical length of an equivalent cylinder dendrite may be measured by adding the electrical lengths of the segments between the "soma" and the dendritic terminals. For the distribution of $R_m$ used here, $L = 1.02$. The calculated transient yielded an $L$ of 1.07 using the 3- and 4-element models. Input resistance may be calculated from the dimensions and specific resistances of the test cell using the method of Rall (1959). This analytical $R_N$ was 1.46 M$\Omega$, while SPICE calculated an $R_N$ of 1.47 M$\Omega$ for the 4-element model and 1.51 M$\Omega$ for the 3-element model. The time constants of such a non-uniform system are not known analytically.

The fidelity with which transients are calculated depends on the frequency response of the system comprised by the SPICE program and the input data. Figure 5 (solid line) shows the frequency response, calculated analytically, of a finite cable with an electrical length of 1.46 and a time constant of 7 ms (see Rall
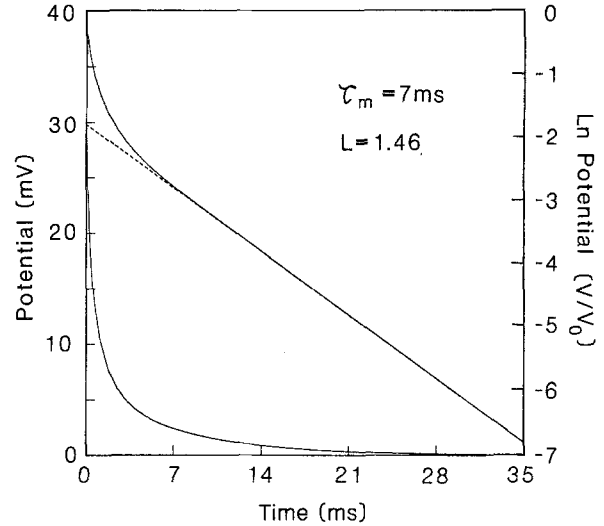


Fig. 3. Voltage transient produced by injecting a brief current pulse in the soma of test-cell 1. The transient is shown on linear (lower solid curve) and semilogarithmic (upper solid curve) scales. The dotted line was fit to the latter part of the transient which showed a single exponential time course of decay. The slope of the dotted line is the time constant, $\tau_m$; $L$ was obtained using Rall's (1969) "peeling" method
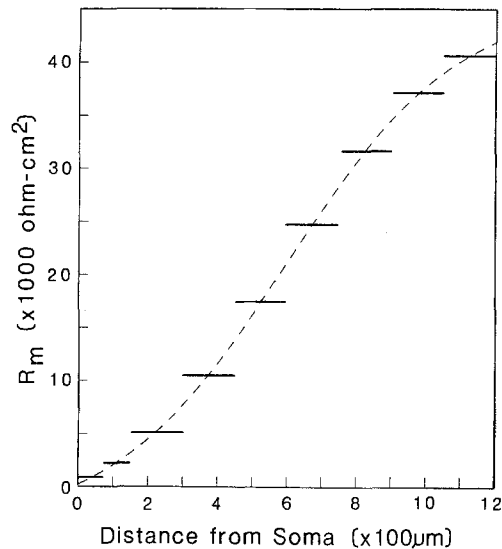


Fig. 4. Assignment of $R_m$ values to dendritic segments of test-cell 1, assuming that $R_m$ increases as a sigmoidal function of distance (dashed curve) along dendritic paths from the soma to individual segments. For example, all dendritic segments between 600 and 750 µm from the soma were assigned $R_m$ values of about $25,000\,\Omega\,cm^2$

1964; Rinzel and Rall 1974; Rall and Segev 1985). Superimposed are Bode plots of test-cell 1 (uniform $R_m$ $= 7000\,\Omega\,cm^2$, other parameters as above) for the 3-element (dotted-dashed line) and 4-element (dashed line) models. These data were obtained using an AC
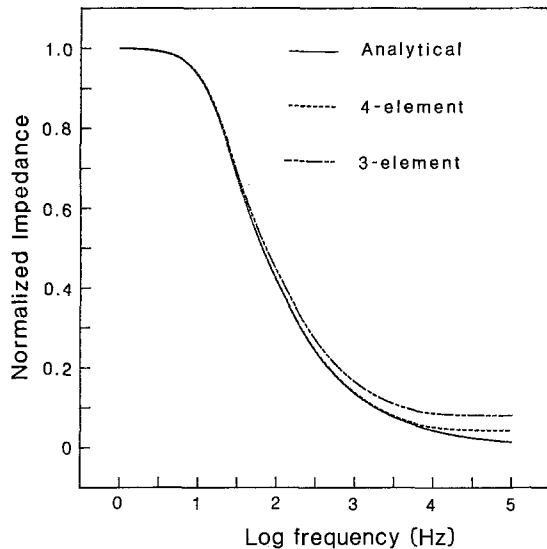
Fig. 5. Frequency response of 3- and 4-element models of test-cell 1, measured at the soma. Note that the 3-element model (long and short dashes) departs from the analytical curve (solid) at a much lower frequency than the 4-element model (short dashes)

analysis mode in SPICE which calculates the response to sinusoidal stimuli over a specified frequency range. In this case, current injection and voltage measurements were done at the "soma" node. The frequency response of the 4-element model is very accurate up to about 10 kHz, while the 3-element model deviates

noticeably from the analytical curve at frequencies as low as 100 Hz.

*3.1.2 Looking from the Dendrites.* As in the case of somatic current injection, when the current source is at a point in the dendritic tree the decay of voltage transients anywhere in the arborization is a sum of infinitely many exponential decays. However, in the latter case, additional fast equalizing time constants, representing the rates at which the current spreads from the point of injection to other branches, appear in the sum. A current transient injected at a terminal produces a local potential that is briefer than the local potential produced by somatic injection of the same current (Rinzel and Rall 1974). Hence, the convergence of the numerical (finite difference) solution to the analytical solution in one case, does not guarantee convergence in the other.

A general analytical result for the case where current in injected at one point in the dendritic tree was derived by Rall and Rinzel (1973; Rinzel and Rall 1974). Parameters of physiological interest, such as input resistance at the current injection site, peak time and peak amplitude of the voltage transient, as well as the transient and steady-state attenuation factors at different locations were tabulated for a specific example (Rinzel and Rall 1974, their Table 1). These parameters were compared to SPICE computations for the same dendritic structure (our test-cell 2) using 3- and 4-element models (Fig. 6 and Table 2). In addition
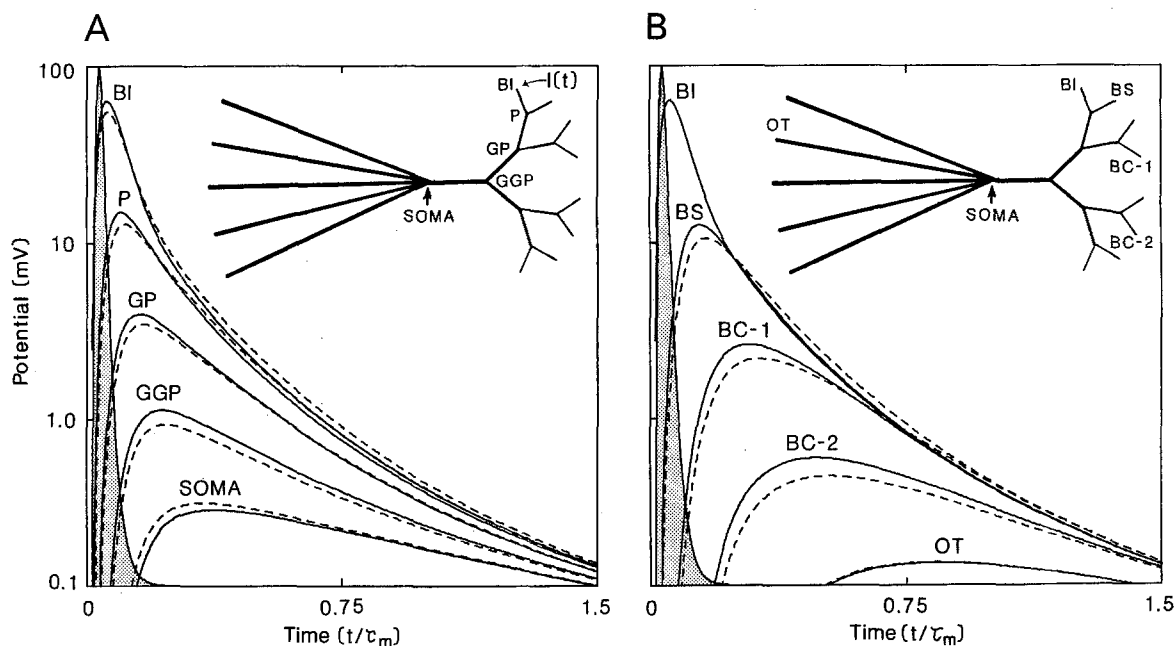


Fig. 6A and B. Response of test-cell 2 (from Rinzel and Rall 1974) to alpha-shaped current injection at dendritic terminal *BI* (insets). Shaded transient shows the time course of the current. Solid and dashed curves show responses of 4- and 3-element models, respectively. A Transients recorded at branch points between *BI* and the soma. B Transients recorded at dendritic terminals

**Table 2.** Comparison between analytical results and SPICE results for 3- and 4-element models of test-cell 2

A. Current injection at a single terminal branch, $BI$[a]

| Location | BI | P | GP | GGP | SOMA | BS | BC-1 | BC-2 | OT |
|---|---|---|---|---|---|---|---|---|---|
| **Peak time** $(t/\tau_m)$ | | | | | | | | | |
| Analytical | 0.040 | 0.085 | 0.135 | 0.210 | 0.350 | 0.120 | 0.270 | 0.460 | 0.840 |
| 3-element | 0.042(+5) | 0.092(+8) | 0.160(+18) | 0.226(+8) | 0.356(+2) | 0.146(+22) | 0.310(+15) | 0.510(+11) | 0.850(+1) |
| 4-element | 0.042(+5) | 0.082(−4) | 0.136(+1) | 0.202(−4) | 0.356(+2) | 0.122(+2) | 0.272(+1) | 0.470(+2) | 0.836(0) |
| **Peak value** (mV) | | | | | | | | | |
| Analytical | 64.8 | 14.5 | 3.75 | 1.05 | 0.276 | 12.8 | 2.54 | 0.557 | 0.135 |
| 3-element | 56.3(−13) | 12.6(−13) | 3.33(−11) | 0.960(−9) | 0.280(+1) | 10.4(−19) | 2.10(−17) | 0.485(−13) | 0.128(−5) |
| 4-element | 64.9(0) | 14.9(+3) | 3.81(+2) | 1.06(+1) | 0.279(+1) | 12.5(−2) | 2.51(−1) | 0.555(0) | 0.136(+1) |
| **Transient attenuation factor** | | | | | | | | | |
| Analytical | 1.0 | 4.5 | 17.3 | 62 | 235 | 5.1 | 25 | 116 | 479 |
| 3-element | 1.0 | 4.5(0) | 16.9(−2) | 59(−5) | 208(−11) | 5.4(+6) | 27(+8) | 116(0) | 440(−8) |
| 4-element | 1.0 | 4.4(−2) | 17.0(−2) | 61(−2) | 233(−1) | 5.2(+2) | 26(+4) | 117(+1) | 477(0) |
| **Steady state attenuation factor** | | | | | | | | | |
| Analytical | 1.0 | 2.3 | 5.3 | 12.0 | 23.9 | 2.4 | 6.0 | 15.5 | 34.0 |
| 3-element | 1.0 | 2.3(0) | 5.4(+2) | 12.0(0) | 23.2(−3) | 2.4(0) | 6.3(+5) | 16.2(+5) | 37.4(+10) |
| 4-element | 1.0 | 2.3(0) | 5.3(0) | 12.0(0) | 23.8(0) | 2.4(0) | 6.04(+1) | 15.6(+1) | 37.0(+9) |

B. Input resistance, electrical length and time constant

| | $R_N$ at soma (MΩ) | $R_N$ at terminal (MΩ) | $L$ value | Normalized $\tau_m$ value |
|---|---|---|---|---|
| Analytical | 1.00 | 15.5 | 1.00 | 1.00 |
| 3-element | 1.05 | 15.1 | 0.99 | 1.00 |
| 4-element | 1.00 | 15.5 | 1.00 | 1.00 |

[a]  Numbers in parentheses are percent errors relative to analytical results

the analytical $R_N$, $L$ and $\tau_m$ values were also compared to values derived from SPICE.

Test-cell 2 was composed of six electrically equivalent dendrites, each with an $L$ of 1.0, originating from a point "soma". The input resistance at the soma was 1 MΩ. One dendrite branched symmetrically every $0.25\lambda$ out to 3rd order terminal branches. The remaining five dendrites were unbranched (Rall and Rinzel 1973; Rinzel and Rall 1974). Since the electrical length criterion was $\Delta X \leq 0.2$, each of the unbranched dendrites were divided into segments of $0.125\lambda$. The branched dendrite was similarly subdivided. In addition, since the analytical results were obtained for a *point* current source, the terminal segment, in which current was injected ($BI$ of Fig. 6), was subdivided into still smaller compartments ($\Delta X = 0.04$; see Discussion). The injected current had an "alpha function" shape with a peak of $10^{-8}$ A and $\alpha = 50$, as in Rinzel and Rall (1974).

Figure 6 shows the potential recorded from branchpoints (Fig. 6A) and terminals (Fig. 6B) after injection of an alpha-shaped current at terminal $BI$. The solid curves are from a 4-element model of test-cell 2, and are virtually superimposable on the analytical curves of Rinzel and Rall (Table 2A). For steady-state calculations the 3-element model is also quite good (see Perkel and Mulloney 1978a), while for fast current transients ($\alpha = 50$) significant errors may occur at some locations in the dendritic tree (dashed lines in Fig. 6). Note that test-cell 2 presents a severe test since the

current is very brief and the injection site is at the extreme tip of a terminal branch. If the current duration were longer and if it were injected at a more proximal location (as in many realistic cases), the differences between the two models should be smaller (see Discussion).

### 3.2 Synaptic Currents

Synaptic input is more accurately represented as an ionic battery acting through a brief synaptic conductance (Eq. (10)), rather than as an independent current source. True synaptic current is not a linear function of the conductance change, due to the dependence of the driving potential on the size of the local membrane potential ($V_m(t) - V_s$ in Eq. (10)), nor is synaptic current proportional to the input resistance at the synapse (Rall 1967). Nonlinear effects also occur when two or more different inputs interact (e.g. Rall 1962, 1964; Burke 1967; Barrett and Crill 1974; Segev and Parnas 1983). It has been suggested that this nonlinearity may be the basis for some integrative processes performed by neurons (Rall 1964; Erulkar et al. 1968; Torre and Poggio 1978; Koch et al. 1983).

Rinzel and Rall (1974) obtained numerical solutions for an analytically derived expression, a linear Volterra integral, which described the voltage pro-
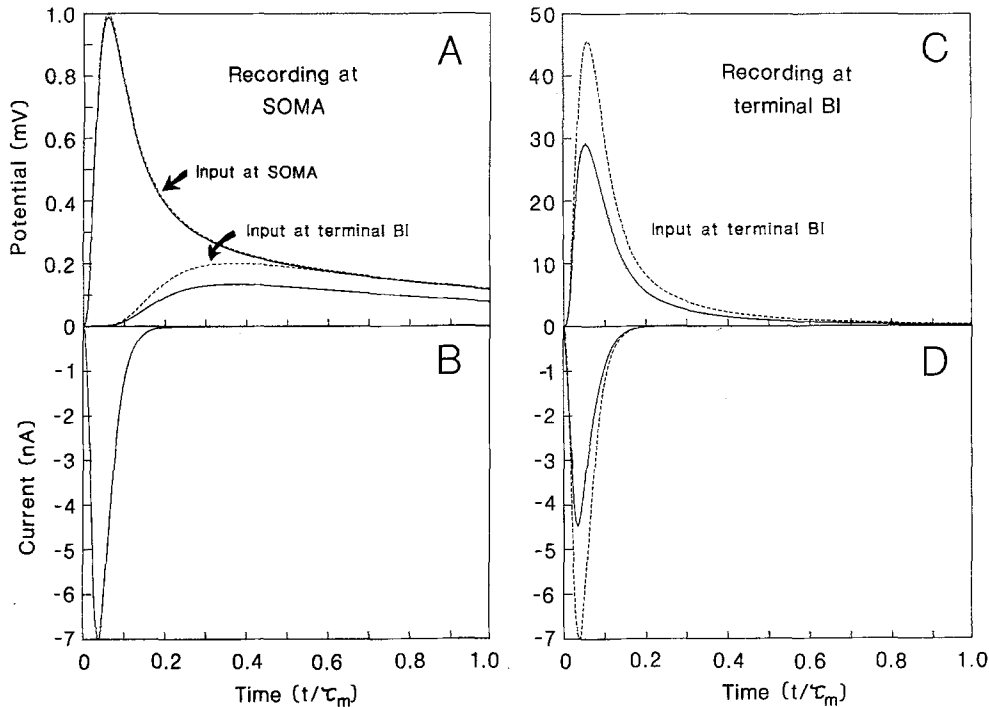
**Fig. 7A–D.** Comparison of potentials (A, C) and currents (B, D) generated in test-cell 2 by a synapse (solid curves) or by an independent current source (dotted curves), both with $\alpha = 50$. A, B Recording from soma, with input at soma and terminal. C, D Recording from terminal with input at terminal

duced by a synaptic input in an idealized neuron (our test-cell 2; see complete derivation in Poggio and Torre 1977). Rinzel and Rall computed the EPSP which resulted from a brief ($\alpha = 50$) conductance change with a peak amplitude of 0.1 μS. Cases where a synapse was located at a dendritic tip or at the soma were compared to "reference" cases where the driving potential was independent of the membrane potential, in other words, setting $V_m(t) = 0$ in Eq. (10). This was accomplished by connecting controlling node 4 in Fig. 2D to ground. To test the nonlinearity inherent in synapses, we have simulated these cases in SPICE and compared them to the analytical results of Rinzel and Rall (1974).

The results obtained from SPICE for the 4-element model are shown in Fig. 7. In all cases the synaptic battery, $V_s$, is 70 mV. When the synapse is on the soma (Fig. 7A, upper pair of curves) the EPSP amplitude is 0.99 mV, compared to 1.00 mV in the reference case. The corresponding values obtained by Rinzel and Rall where 0.97 and 0.98 mV, respectively. The peak synaptic current calculated by SPICE was 6.91 nA (Fig. 7B). As expected for such a small change in the driving potential, the difference between the synaptic potential and the reference potential is negligible.

With the same input at terminal *BI*, large differences between the two cases were observed. The EPSP amplitude at the synapse was 29.5 mV (compared to 28.8 mV calculated by Rinzel and Rall). The

value in the reference case is 46.6 mV (Fig. 7C, continuous line vs dashed line). The associated peak currents are 4.68 nA and 7.00 nA respectively (Fig. 7D; compare with a peak synaptic current of 4.77 nA expected analytically). These differences result from the large local EPSP and the consequent reduction in synaptic driving potential. The somatic voltage transient produced by synaptic current and the independent "reference" current injected at terminal *BI* are shown in Fig. 7A (lower pair of curves). A somatic peak amplitude of 0.133 mV was generated by the synapse (continuous line; compare with the analytical value of 0.129 mV) and a 0.2 mV potential was produced by the independent current source (dashed line). This 33.5% decline in peak somatic EPSP amplitude relative to the reference potential may be compared with a value of 32.8% obtained by Rinzel and Rall. These results confirm that the model for a synaptic input as shown in Fig. 2D is accurate and that the SPICE solution converges to the correct solution when a complex dendritic system is perturbed by a brief conductance change.

## 4 Discussion

The advantage of compartmental models of neurons over analytical ones is that they may handle situations too complex to be solved exactly. In principle, analyt-

ical solutions to the cable equations can be obtained for neurons with arbitrarily complex dendritic structure, provided the membrane is passive. For this purpose, Rall's algorithm (1959) can be used (Barrett and Crill 1974; Turner 1984), as well as the algorithm of Butz and Cowan (1974; see also Horwitz 1981, 1983; Koch and Poggio 1983; for a different analytical approach see Poggio and Torre 1977). However, when such a passive system is perturbed by a large number of synaptic inputs the analytical solution becomes impractical. If the system includes compartments with excitable membrane, analytical solutions do not exist. For these cases a compartmental model is a necessary tool for a correct interpretation and understanding of the neuron's electrical behavior (Rall 1964).

It should be remembered that a compartmental model approximates the continuous (analytical) problem by finite, discrete, isopotential compartments. In mathematical terms, the continuous cable equation is discretized into a set of finite difference equations. The number of compartments necessary to obtain a satisfactory approximation to the continuous case is determined both by the demands of the specific anatomy as well as by numerical considerations (see below). For example, the morphology of the six motoneurons analyzed in the study of Fleshman et al. (in preparation) was adequately represented by 500–800 segments. Additional subdivision of segments necessitated by the maximum electrical length criterion typically resulted in a total of 800–1200 compartments for each cell.

## 4.1 Anatomical Considerations

The nomenclature system described in the model formulation section embodies an algorithm which has proven useful in uniquely naming and correctly connecting large numbers of dendritic segments. The simple expedient of numbering branches of asymmetrical dendrites as though they were fully symmetrical (i.e. reserving the numbers of "missing" branches) allows one to encode the precise location of a segment within a complex arborization. From the name of a segment it is easy to deduce the names of its parent and grandparent branches all the way back to the soma and the names of all possible daughter branches. We have used this algorithm in a computer program which takes as input the name, length and diameter of an anatomical segment, and the chosen $R_m$, $R_i$, and $C_m$ values, and outputs appropriately formatted SPICE code representing the segment. The program also divides and renames the dendritic compartments according to a $\Delta X$ criterion.

In practice this method may be used to represent branching structures which are not strictly binary. For instance, infrequent trifurcations may be approximated by two very close bifurcations. A dendritic spine may be modelled as a short branch with one or more compartments representing its neck and another, a simple R–C compartment, representing the head. For branching patterns that are intrinsically not binary, a different naming scheme would be more useful.

An important question in constructing models of real neurons is: how faithfully must be anatomical structure be approximated by a compartmental model? This question arises when the morphology being simulated is very irregular, for example, where dendrites are varicose or laden with spines. In these cases, accurate representation of the anatomy may require a huge number of compartments. Usually such a refinement of the compartmental model has a very small effect on measurements of the neuron's electrical properties as seen from the soma. However, if local interactions in the dendrites are of interest (between two adjacent synapses for example), a more detailed representation of the region of interest may be very important. Similar reasoning led us to make additional subdivisions in the tip-most compartment of test-cell 2, in order to more accurately simulate a point current source.

## 4.2 Numerical Considerations

In general, a compartmental model converges to the analytical solution as the number of compartments increases. This in turn will rapidly increase the demand for computer storage space and computation time. The accuracy of the computation depends on the parameter of interest and on the circuit chosen to represent single compartments.

As we have illustrated, the distributed resistances and capacitance of an anatomical segment may be lumped to form a single compartment in two different ways (Fig. 2B, C). When anatomical segments are represented by either a 3- or 4-element compartment, differences in model behavior occur in steady state and transient calculations even though the actual values of CM, RM and total $RI$ for each compartment are the same in both cases (see Table 2).

The 4-element model requires four connecting nodes while the 3-element model uses only three (Fig. 2B, C). This difference results in a matrix of first order differential equations for the 3-element model that has one third fewer rows than the 4-element model. These differential equations have to be solved for each time step, and as noted above, for complex structures SPICE may converge much faster with the 3-element representation than with the 4 element representation.

A necessary step to assess the accuracy of these two compartmental models is to compare their behavior to

analytical results. A thorough comparison of this kind was done for the 3-element compartment by Perkel and Mulloney (1978a). They found that the steady-state attenuation factor between the ends of a compartmentally modeled cable, with $L=1.5$ and $\Delta X=0.2$ is about 10% less than the analytical value (their Table 1). This is also the case in our computations using the 3-element model (Table 2, between $BI$ and $OT$). For an intermediate point, such as the soma, we found smaller deviations from the analytical solution. The computations of Perkel and Mulloney for transients resulting from instantaneous current injection yielded shape parameters compatible with our 3-element model for the case of $\Delta X=0.2$ (Table 2).

Intracellular recordings from cat spinal $\alpha$-motoneurons most likely result from microelectrode penetration in the soma or in a thick dendritic trunk that is electrically very close to the soma (Burke and Rudomin 1977). With a bridge circuit it is possible to inject current through the somatic electrode and measure the resulting potential. Transients resulting from a brief somatic current pulse should contain at least the two slowest analytical time constants, $\tau_0$ and $\tau_1$; $\tau_0$ is a direct measure of the membrane time constant and the electrical length may be obtained from their ratio (Rall 1969). With a long current pulse, the ratio of the steady state potential to the current magnitude is a measure of input resistance.

Therefore, for the case of somatic stimulation and recording, a compartmental model may be considered accurate if the correct membrane time constant, electrical length and input resistance, are obtained. Dendrites as complicated as those of $\alpha$-motoneurons may affect the accuracy of the SPICE computation, as well as increasing the requirements for CPU time. From our studies using test-cell 1, a model with almost 1200 compartments, we may conclude that the 3-element model, with $\Delta X \leq 0.2$, is a reasonable model. For six $\alpha$-motoneurons we have simulated in a separate study, the 3-element model with $\Delta T=0.01\tau_m$ and a total analysis duration of $5\tau_m$ (i.e. 500 points) yielded somatic transients after 10 min to 2 h of CPU time. The same transients produced using the 4-element model required 2–30 h of CPU time, while differences between the models in $\tau_m$, $L$ and $R_N$ were less than 5%.

To study the characteristics of synaptic input it is essential to obtain the correct shape parameters of the voltage perturbation recorded at the soma. Unlike the steady-state case, these parameters are very dependent on the way in which the lumped membrane impedance is distributed in the 3- and 4-element models.

The peak voltage produced at the soma by injection of an alpha-shaped current at a dendritic terminal is very similar in both models and accurate within 2% of the analytical results for $\Delta X \leq 0.2$ (Table 2, peak

value at soma). However, the 3-element model significantly underestimates (11%) the attenuation factor by which the voltage transient amplitude is reduced by electrotonic spread from the terminal to the soma. This discrepancy is greatly reduced when the location of the synapse is more proximal or when the current duration is increased. With increased current duration, the behavior of the system becomes more like the steady-state case. We conclude that the 3-element model, with $\Delta X \leq 0.2$, is a reasonable representation when the final amplitude at the soma is the parameter of interest. The situation may be quite different, however, if one is interested in the degree of attenuation between the synapse and the soma or in the potential amplitude at other locations in the dendritic tree.

For example, using the 3-element model, injecting the alpha current at terminal segment $BI$ of test-cell 2 (Table 2) produces a transient in the soma only 1% larger than the analytical result. However, the transient recorded at terminal segment $BS$, adjacent to $BI$, is 19% smaller than the analytical result. The size and shape of the transient at different locations in a dendritic tree are crucial when nonlinear interactions may occur, as with multiple synapses or repetitive activation of single synapses. In these situations, even small errors in the calculation of individual EPSPs may lead to serious errors in the overall response (Rall 1964; Koch et al. 1983; Segev and Parnas 1983). Therefore, in studies of interactions between dendritic synapses, the 4-element model is the most appropriate.

### 4.3 Further Possibilities

SPICE may be used to simulate nonlinear membrane properties using methods similar in principle to those described for modeling synaptic input. The following paper (Bunow et al. 1985) presents detailed techniques for implementing Hodgkin-Huxley-like active conductances in SPICE.

### References

Barrett JN, Crill WE (1974) Specific membrane properties of cat motoneurones. J Physiol 239:301–324

Brown TH, Fricke RA, Perkel DH (1981) Passive electrical constants in three classes of hippocampal neurons. J Neurophysiol 46:812–827

Bunow B, Segev I, Fleshman IW (1985) Modeling the electrical behavior of anatomically complex neurons using a network analysis program: Excitable membrane. Biol Cybern 53:41–56

Burke RE (1967) Composite nature of the monosynaptic excitatory postsynaptic potential. J Neurophysiol 30:1114–1137

Burke RE, Rudomin P (1977) Spinal neurons and synapses. In: Kandel ER (ed) Handbook of physiology. The nervous system. Sect 1. Vol 1, Pt 2, Bethesda: Am Physiol Soc pp 877–944

Butz EG, Cowan JD (1974) Transient potentials in dendritic systems of arbitrary geometry. Biophys J 14:661–689

Cooley JW, Dodge FA (1966) Digital computer solutions for excitation and propagation of the nerve impulse. Biophys J 6:583–599

Cullheim S, Fleshman JW, Glenn LL, Burke RE (1985) Membrane area and dendritic structure of type-identified triceps surae motoneurons. Submitted for publication

Cullheim S, Kellerth J-O (1976) Combined light and electron microscopic tracing of neurons, including axons and synaptic terminals, after intracellular injection of horseradish peroxidase. Neurosci Lett 2:307–313

Edwards DH, Mulloney B (1984) Compartmental models of electrotonic structure and synaptic integration in an identified neurone. J Physiol 348:89–113

Erulkar SD, Butler RA, Gerstein GL (1968) Excitation and inhibition in cochlear nucleus. II. Frequency modulated tones. J Neurophysiol 31:537–548

Goldstein SS, Rall W (1974) Changes in action potential shape and velocity for changing core conductor geometry. Biophys J 14:731–757

Horwitz B (1981) An analytical method for investigating transient potentials in neurons with branching dendritic trees. Biophys J 36:155–192

Horwitz B (1983) Unequal diameters and their effects on time-varying voltages in branched neurons. Biophys J 41:51–66

Jack JJB, Redman SJ (1971) The propagation of transient potentials in some linear cable structures. J Physiol 215:283–320

Jankowska E, Rastad J, Westman J (1976) Intracellular application of horseradish peroxidase and its light and electron microscopical appearance in spinocervical tract cells. Brain Res 105:557–562

de Jongh HR, Kernell D (1982) Limits of usefulness of electrophysiological methods for estimating dendritic length in neurones. J Neurosci Meth 6:129–138

Khodorov BI (1974) The problems of excitability. Dodge FA (ed), Translated by Haigh B Plenum New York

Koch C, Poggio T (1983) A theoretical analysis of electrical properties of spines. Proc R Soc (London B) 218:455–477

Koch C, Poggio T, Torre V (1983) Nonlinear interaction in dendritic tree: Localization, timing and role in information processing. Proc Nat Acad Sci 80:2799–2802

Knott GD (1979) MLAB – a mathematical modeling tool. Comp Prog Biomed 10:271–280

Moore JW, Ramon F, Joyner RW (1975) Axon voltage-clamp simulations. Biophys J 15:11–69

Parnas I, Segev I (1979) A mathematical model for conduction of action potentials along bifurcating axons. J Physiol 295:323–343

Perkel DH, Mulloney B (1978a) Electrotonic properties of neurons: Steady-state compartmental model. J Neurophysiol 41:627–639

Perkel DH, Mulloney B (1978b) Calibrating compartmental models of neurons. Am J Physiol 235 (Reg Int Comp Physiol 4):R93–R98

Poggio T, Torre V (1977) A new approach to synaptic interactions. In: Heim H, Palm G (eds) Lecture notes in biomathematics. vol 21. Theoretical approaches to computer systems, vol. 21, Springer, Berlin Heidelberg New York, pp 89–115

Rall W (1959) Branching dendritic trees and motoneuron membrane resistivity. Exp Neurol 1:491–527

Rall W (1960) Membrane potential transients and membrane time constant of motoneurons. Exp Neurol 2:503–532

Rall W (1962) Theory of physiological properties of dendrites. Ann NY Acad Sci 96:1071–1092

Rall W (1964) Theoretical significance of dendritic trees for neuronal input-output relations. In: Reiss RF (ed) Neural Theory and Modelling. Stanford University Press, Stanford, pp 73–97

Rall W (1967) Distinguishing theoretical synaptic potentials computed for different soma-dendritic distributions of synaptic input. J Neurophysiol 30:1138–1168

Rall W (1969) Time constants and electrotonic length of membrane cylinders and neurons. Biophys J 9:1483–1508

Rall W (1977) Core conductor theory and cable properties of neurons. In: Kandel ER (ed) Handbook of physiology. The nervous system. Sect. 1, vol 1, pt 1, Bethesda: Am Physiol Soc pp 39–97

Rall W, Rinzel J (1973) Branch input resistance and steady attenuation for input to one branch of a dendritic neuron model. Biophys J 13:648–688

Rall W, Segev I (1985) Space clamp problems when voltage clamping branched neurons with intracellular microelectrodes. In: Smith TG Jr, Lecar H, Redman SJ, Gage PW (eds) Voltage clamping and patch clamping with microelectrodes Bethesda: Am Physiol Soc pp 191–215

Rall W, Shepherd GM (1968) Theoretical reconstruction of field potentials and dendrodendritic synaptic interactions in olfactory bulb. J Neurophysiol 31:884–915

Rall W, Burkey RE, Smith TG, Nelson PG, Frank K (1967) Dendritic location of synapses and possible mechanisms for the monosynaptic EPSP in motoneurons. J Neurophysiol 30:1169–1193

Rinzel J, Rall W (1974) Transient response in a dendritic neuron model for current injected at one branch. Biophys J 14:759–790

Segev I, Parnas I (1983) Synaptic integration mechanisms: A theoretical and experimental investigation of temporal postsynaptic interactions between excitatory and inhibitory inputs. Biophys J 41:41–50

Shelton DP (1985) Membrane resistivity estimated for the Purkinje neuron by means of a passive computer model. Neurosci 14:111–131

Shepherd GM, Brayton RK (1979) Computer simulation of a dendro-dendritic synaptic circuit for self- and lateral-inhibition in the olfactory bulb. Brain Res 175:377–382

Torre V, Poggio T (1978) A synaptic mechanism possibly underlying directional selectivity to motion. Proc R Soc (London B) 202:409–416

Traub, RD, Llinas R (1979) Hippocampal pyramidal cells: Significance of dendritic ionic conductances for neuronal function and epileptogenesis. J Neurophysiol 42:476–496

40

Turner DA (1984) Segmental cable evaluation of somatic tran-
sients in hippocampal neurons (CA1, CA3, and dentate).
Biophys J 46:73–84

Ulfhake B, Kellerth J-O (1981) A quantitative light microscopic
study of the dendrites of cat spinal $\alpha$-motoneurons after
intracellular staining with horseradish peroxidase. J Comp
Neurol 202:571–583

Vladimirescu A, Zhang K, Newton AR, Pederson DO,
Sangiovanni-Vincentelli A (1981) SPICE version 2G User's
guide. EECS Department University of California, Berkeley

Dr. J. W. Fleshman
Laboratory of Neural Control
National Institute of Neurological
and Communicative Disorders and
Stroke, Bldg. 36, Rm 5A29
National Institutes of Health
Bethesda, MD 20205
USA